Biosensors and Bioelectronics 42 (2013) 80–86

Contents lists available at SciVerse ScienceDirect

Biosensors and Bioelectronics

journal homepage: www.elsevier.com/locate/bios

Construction of a novel macroporous imprinted biosensor based on quartz crystal microbalance for ribonuclease A detection

Shuai Liu, Dezhong Zhou, Tianying Guo*

Key Laboratory of Functional Polymer Materials (Nankai University), Ministry of Education, Institute of Polymer Chemistry, College of Chemistry, Nankai University, Weijin Road, No. 94, Tianjin 300071, China

ARTICLE INFO

Article history:
Received 23 September 2012
Received in revised form
31 October 2012
Accepted 1 November 2012
Available online 7 November 2012

Keywords:
QCM
Protein imprinted films
Macroporous
Fluoromonomer
N-methacryloyl-histidine

ABSTRACT

A novel quartz crystal microbalance (QCM) biosensor with high selectivity and sensitivity has been developed for ribonuclease A determination. Macroporous protein imprinted films have been fabricated on the surface of QCM electrode using 2,2,3,4,4,4-hexafluorobutyl methacrylate (HFBMA) as the main matrix monomer, N-methacryloyl-histidine (MAH) as the functional monomer, and trimethylolpropane trimethacrylate (TRIM) as the cross-linker. The imprinted special surface area and the quantity of the imprinted sites were increased by the formation of macropores that were generated by employing calcium carbonate nanoparticles as the porogen. The selectivity factor was improved obviously for the fluoromonomer containing system, especially in dilute protein solution, which gets benefit from the reducing of the nonspecific adsorption of proteins. Furthermore, MAH can not only play the role as the functional monomer, but also improve the hydrophilicity of surface of the imprinted film, which makes for the adsorption of proteins. At last, the rigid skeleton structure made the films durable in the recycled tests.

1. Introduction

In the recent years, there has been a growing interest in molecular sensors demonstrating not only high specificity, sensitivity, and quick response, but also easy regeneration and use in analyte detection, medical diagnostics, stimulant control and drug delivery (Yano and Karube, 1999; Byren and Dianmond, 2006; Potyrailo, 2006; Sellergren and Allender, 2005). Although some progresses have been made towards improving the performances of sensors, it is still a challenge to find an efficient way to construct an extensively practicable sensor that simultaneously possesses all these desirable features rather than improving one feature at the expense of another.

With the development of biotechnology and modern electronics, quartz crystal microbalance (QCM) sensors, due to their less sample consumption and simple operation, have been widely used because of their high sensitivity, label-free, shorter analysis time and real-time analysis (Jonsson et al., 2008). For a rigid, uniform and thin-film layer, the oscillation frequency shift is directly proportional to the mass change on the surface of quartz crystal, which makes the QCM an increasingly popular platform for biosensor applications (Aizawa et al., 2004). In the recent years, the combination of QCM with molecular imprinting (MIP) technology for molecular recognition has attracted much attention (Cui et al., 2000; Lee and James, 2011).

Molecular imprinting is a promising technique for analyte detection. Although small molecule imprinting has been straightforward now (Wang et al., 2006; Pernites et al., 2011; Li et al., 2011), demands for recognition of macromolecules, such as DNA and proteins, are continually growing in recent years (Xia et al., 2005; Guo et al., 2004; Bossi et al., 2007; Cutivet et al., 2009; Zhang et al., 2011). But the major problem associated with the imprinting of proteins lies in their restricted mobility within highly cross-linked polymer networks and the poor efficiency in rebinding (Lu et al., 2012). Meanwhile, the flexible structure, easy denaturation and large size of proteins will hinder them from reaching and leaving binding sites. Thereupon, surface imprinting has been developed to overcome these problems (Tan et al., 2008).

During protein imprinting process, methacrylic acid (MAA) and acrylamide (AAM) are usually used as the functional monomers, because the "soft" character imparts the imprinted hydrogel matrices good conformation adaptability to the protein. However, disadvantages such as the structure instability and poor mechanical properties limit their practical application. So rigid organic polymer or organic/inorganic hybrid material was reconsidered by many researchers (Tan and Tong, 2007; Tatemichi et al., 2007). In our prior work, the rigid monomer methyl methacrylate (MMA) was also used as the main matrix (Zhou et al., 2011). The interactions between template protein and the

* Corresponding author. Tel./fax: +86 22 23501597.
E-mail address: tyguo@nankai.edu.cn (T. Guo).

0956-5663/$ - see front matter © 2012 Elsevier B.V. All rights reserved.
http://dx.doi.org/10.1016/j.bios.2012.11.002

MMA matrix are mainly based on the hydrophobic interaction, which is quite strong compared to other interactions such as hydrogen bond and ion interaction in aqueous environment. However the hydrophobic interaction does not have specificity, which would negatively interfere with the recognition properties (Bures et al., 2011). Thus a considerable reduction for the hydrophobic interaction between the MIP surface and the template is required, which was achieved through the introduction of hydrophilic components and this also would lead to a relatively higher selectivity of the material (Yang et al., 2011).

As we know, fluoropolymers have many unique characteristics such as high hydrophobicity, high thermal and mechanical stability, oil and water-repellency, and very interesting surface properties (Liu et al., 2012). So to reduce nonspecific adsorption and fabricate a rigid structure, 2,2,3,4,4,4-hexafluorobutyl methacrylate (HFBMA) was selected as the main matrix monomer. The fluorine-containing segments, due to their low surface free energy, would be prone to gather on the solid-air interface, forming an excellent protein barrier during application (Ernsting et al., 2007; Kwon et al., 2011; Zhang et al., 2012). Unlike acrylate based polymer as the monomer, the presence of fluorinated groups would lessen the nonspecific adsorption due to protein repulsion behavior. On the other hand, N-methacryloyl-histidine (MAH) was introduced as the functional monomer, which would enlarge the specific binding affinity to the target protein because of electrostatic interactions between MAH and proteins in neutral solutions. As far as we know, there are not related reports on protein imprinted film with the balance of reduced nonspecific adsorption and enhanced specific adsorption based on QCM sensor by now.

In this special system, imprinted films are fabricated in situ on the surface of QCM electrode. Once target molecules are adsorbed into the imprinted cavities, the oscillation frequency decreases. However the oscillation frequency shift usually derives from both mass change on the electrode and viscoelasticity variation at interface. But for a rigid system, the mass change is directly proportional to the frequency shifts and can be estimated more directly and efficiently. As a piezoelectric acoustic sensor, QCM has high sensitivity, but the efficient surface area of the electrode is so small that leads to a relatively low adsorption capacity and compromises the detection sensitivity. Consequently, increasing the specific surface area of sensing materials is a facile approach to further improve the sensitivity of QCM sensors (Zheng et al., 2008). For example, Ding et al. (2011) developed a polyethyleneimine (PEI) modified electrospun polystyrene (PS) (PEI-PS) nanoporous fibers coated QCM sensor to enhance formaldehyde sensing. In our previous work, calcium carbonate nanoparticles were used as the porogen in the preparation of imprinted film and performed excellent porous effect (Zhou et al., 2011). Thus, this method was still utilized to this new material system.

2. Experimental

2.1. Materials

2,2,3,4,4,4-hexafluorobutyl methacrylate (HFBMA, Xeogia Fluorine-Silicon Chemical, Harbin, China), butyl Methacrylate (BMA, Tianjin Chemical Reagent Institute, China) and trimethylolpropane trimethacrylate (TRIM, Tianjin Chemical Reagent Institute, China) was vacuum distilled prior to use. N-methacryloyl-histidine (MAH) was prepared as the reference (Say et al., 2002) and the ^{1}H NMR data are that δ_{ppm}: 5.36 (s, 1H), 5.45 (s, 1H), 6.97, 6.94 (d, 1H), 7.70, 7.68 (d, 1H) and the yield is about 53%. Darocur 1173 was purchased from Ciba Specialty Chemicals Co. Ltd (China). Ribonuclease A (pI=7.8, M_w=13,700) from bovine pancreas and Lysozyme (pI=11.2, M_w=14,300) from chicken egg white were purchased from Beijing Dingguo Biotech. Co. Ltd. (China). Phosphate buffer solution (PBS, pH=7.2, 0.05 M) was purchased from Lianxing Biotech. Co. Ltd. (China). Calcium carbonate nanoparticles (15–40 nm in diameter) were gained from Nanomaterials Technology Co. Ltd. (China).

2.2. QCM apparatus

The Quartz Crystal Microbalance (QCM200) from Stanford Research Systems, Inc. (USA) is composed of Crystal Holder, Oscillator Module, Frequency Counter and PC interface connection for signal output visualization. A 5 MHz AT-cut piezoelectric quartz wafer (2.54 cm in diameter) attached with two gold electrodes (0.40 cm^2 active oscillation area) on both sides was used as the transducer of the QCM biosensor of this study. The crystal was placed in the holder and positioned by two O-rings so that one side of the electrodes was exposed to the sample solution. The measurement chamber formed by the Teflon holder and flow cell was about 150 μL. And the crystal oscillation signal readout was recorded by QCM software installed on a host personal computer.

2.3. Preparation of ribonuclease A imprinted macroporous (porous-HFBMA-MAH-MIP) film

Prior to use, quartz wafer was first rinsed with deionized water and ethanol for three times respectively and dried under gentle nitrogen flow atmosphere. The freshly cleaned chip was dipped into allyl mercaptan solution overnight, the gold electrode was then washed with ethanol and deionized water to remove excess thiols and dried under nitrogen.

To get 4.0 mg/mL calcium carbonate nanoparticles suspension, 200.0 mg calcium carbonate nanoparticles were dispersed into 50.0 mL anhydrous ethanol through high-speed shearing at 5000 rpm for 5 min and ultrasonic vibration for 10 min. Then a clean round glass coverslip (12 mm in diameter and treated with trimethylchlorosilane solution beforehand) was dipped into the nanoparticles suspension, taken out vertically with a steady pace, placed flat and dried at ambient temperature. After 20 times of above operation, the coverslip was covered with a white layer of calcium carbonate nanoparticles. Dropping 50 μL of ribonuclease A phosphate buffer solution (25 mg/mL) onto the nanoparticles layer, the white layer became transparent, indicating the successful infiltration of protein solution. Then the coverslip was subjected to spin-coating at 600 rpm for 18 s and 5000 rpm for 30 s. Twice the dropping and spin-coating operation, then repeat the above procedure with MAH phosphate buffer solution (50 mg/mL). Afterwards, 2 μL of homogeneous mixture of HFBMA (160 μL), TRIM (80 μL) and 1173 (10 μL) was dropped onto the nanoparticles/template/MAH layer. Once again the layer became transparent, and a 5 MHz AT-cut quartz crystal electrode was covered on the top of the polymer precursors. Then the sandwich (glass coverslip/calcium carbonate nanoparticles layer/template protein/MAH/ polymer precursors/quartz crystal electrode) was exposed to UV light (365 nm, 1200 W, 50 cm high, every 30 s UV exposure following by 10 min cooling) to photopolymerize for 1 min under nitrogen atmosphere. After polymerization, the glass coverslip was peeled off and the sandwich (calcium carbonate nanoparticles layer/template protein/MAH/polymer precursors/quartz crystal electrode) was dipped into 2% hydrochloric acid solution for 0.5 h to fully dissolve the calcium carbonate nanoparticles. The obtained complex layer (protein imprinted polymer film/quartz crystal electrode) was washed with sodium chloride solution (3 M) for at least 10 h in order to remove the template completely. The obtained macroporous imprinted film was then

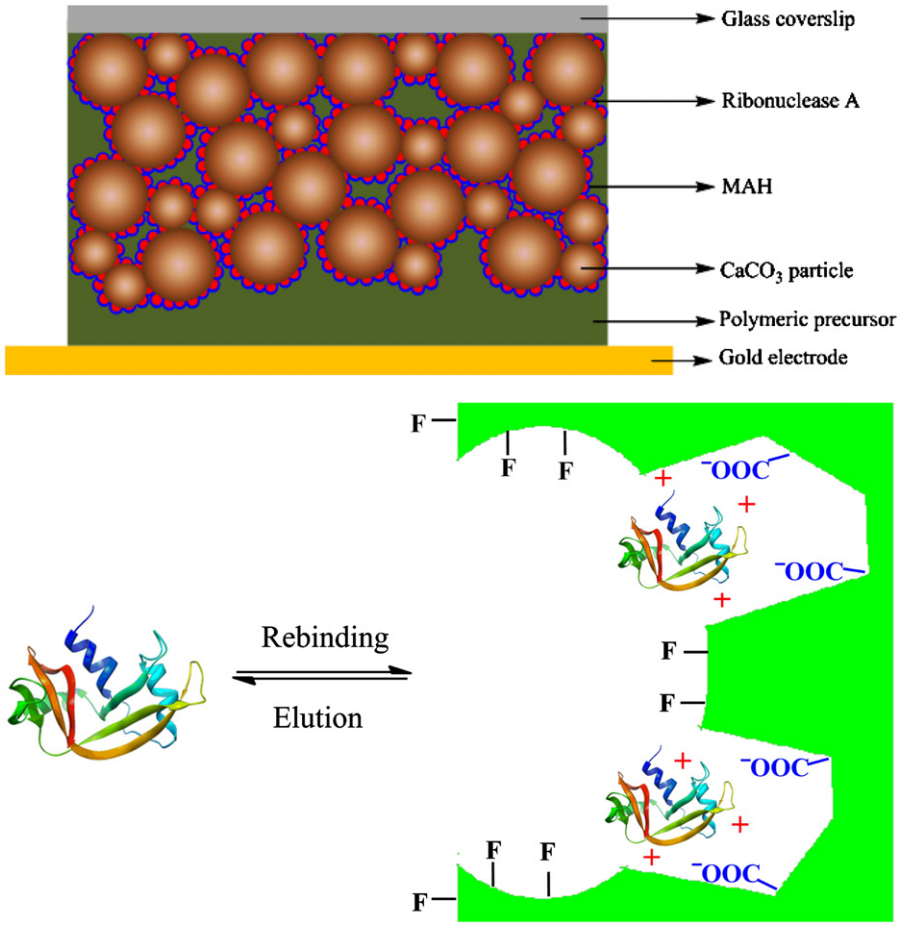

Scheme 1. Schematic illustration for the structure of macroporous protein surface imprinted film coated on a QCM electrode and the microcosmic interactions between protein and matrix in the macropore.

washed with deionized water and maintained in phosphate buffer solution (PBS, pH=7.2, 0.05 M) for protein assays. The structure of macroporous protein surface imprinted film is illustrated in Scheme 1.

The film using BMA as the main matrix monomer (porous-BMA-MAH-MIP) was also prepared in the same way as above. The nonimprinted macroporous (porous-HFBMA-MAH-NIP) film, the imprinted nonporous (nonporous-HFBMA-MAH-MIP) film and the imprinted macroporous (porous-HFBMA-MIP) film without MAH were fabricated in the same way except the presence of template, porogen and MAH respectively.

2.4. QCM measurements

Different films were prepared on quartz crystal electrode respectively and transferred to the chamber of the 5 MHz quartz crystal microbalance. Before each protein binding experiment, the crystal electrode was immersed in the phosphate buffer solution to equilibrate as long as possible to reduce the long-term frequency shifts. For the resonance tests, the basic oscillation frequency was first recorded (f_0), while it was stabilizing within ± 2 Hz in 30 min in phosphate buffer solution. Then 150 μL of ribonuclease A sample in different concentrations (1×10^{-6}, 1×10^{-5}, 5×10^{-5}, 1×10^{-4}, 5×10^{-4}, 1×10^{-3} g/mL) was injected into the flow cell at a steady fast speed and the tests were conducted under the static condition afterwards. After 30 min of each injection, the oscillation frequency was recorded again (f_i) and the frequency shift could be calculated ($\Delta f_i = f_i - f_0$). Then 10 mL of sodium chloride (0.5 M) phosphate buffer solution (pH=7.2, 0.05 M, denoted as the elution solution) was injected into the chamber to elute the adsorbed protein. Followed with phosphate buffer solution injection until the QCM oscillation frequency was back to the basic frequency. For the selectivity tests, lysozyme was dissolved in phosphate buffer solution (PBS, pH=7.2, 0.05 M) and the measurements were conducted in analogy to that of ribonuclease A sample did. For each test, the capacitance cancellation was checked and readjusted. All the measurements were carried out at 21 °C.

The imprinting specificity of a MIP is evaluated by the selectivity factor (SF), which is defined as follows:

$$SF = \Delta f_{i\text{-template}} / \Delta f_{i\text{-control}} \quad (1)$$

where $\Delta f_{i\text{-template}}$ is the Δf_i of the MIP film for template protein and $\Delta f_{i\text{-control}}$ is the Δf_i of the MIP film for control protein.

2.5. Characterization

^{1}H NMR spectrum was recorded on a Varian UNITY-plus 400 spectrometer with D20 as the solvent.

The surface morphologies of films were investigated by scanning electron microscopy (SEM, ZEOLZSM6700F, Japan).

Water contact angles (WCA) were measured with Dataphysics OCA ISEC contact angle meter (German). A droplet of deionized water was placed on the polymeric thin film, and the contact angle was measured by video imaging, using the "circle method".

Elemental analyzer (vario EL CUBE, German) was used to characterize the composition of the copolymer films.

3. Results and discussion

3.1. Design of the imprinted film materials

In recent years, much progress has been made in constructing surface protein imprinted polymers using acrylate materials as the monomer (Tan and Tong, 2007; Tatemichi et al., 2007; Zhou et al., 2011). However, the nonspecific interactions between protein and acrylate are so strong, that may interfere with the imprinting effect. Through surface hydrophilic modification, the nonspecific interactions between protein and acrylate can be lessened (Yang et al., 2011; Hua et al., 2011). But the effect is not outstanding, the possible reason is that though the nonspecific adsorption decreases after the introduction of hydrophilic interactions, meanwhile specific adsorption originate from hydrophobic interactions also decreases obviously. Accordingly the selectivity was improved at the expense of decreased adsorption capacity. Thus seeking more desirable material design proposal is a significant theme all the while. Fluorine-containing materials are selected as the matrix which exhibit stronger hydrophobicity compared to acrylate based matrix. Whereas fluoropolymers have the property of protein-repellency, thereby the problem of strong nonspecific adsorption due to hydrophobic interactions can be overcome. To introduce specific interactions, hydrophilic functional monomer MAH was designed and prepared in our work, which made the protein easier to approach the surface of the fluorine-containing hydrophobic matrix. To investigate the hydrophilicity of the imprinted films after MAH introduction, the water contact angles of three different kinds of films porous-HFBMA-MIP, porous-HFBMA-MAH-MIP and porous-BMA-MAH-MIP were measured. As Fig. S1 showed, the water contact angle of porous-HFBMA-MIP film was as high as 110.4°, exhibiting a strong hydrophobic feature. However, the water contact angles of porous-HFBMA-MAH-MIP and porous-BMA-MAH-MIP films were 62.0° and 57.8° respectively. An obvious decrease in contact angle was observed after MAH introduction, indicating that MAH can enhance the hydrophilicity of the film largely. This is also an evidence that MAH has been grafted to the surface of the film. And the elemental analysis showed that the contents of N atom were 1.7% and 2.2% for porous-BMA-MAH-MIP and porous-HFBMA-MAH-MIP films respectively, while no N atom existed in porous-HFBMA-MIP film. And this also indicates the effective MAH introduction of the film.

3.2. Film morphology effect on template assay

To prepare the rigid porous-HFBMA-MAH-MIP film on QCM electrode for protein recognition, calcium carbonate nanoparticles (15–40 nm in diameter) were selected as the porogen. Scanning electron microscopy was used to capture the microscopic images of the films. Fig. 1a and b are the morphological images of the porous-HFBMA-MAH-MIP film and the counterpart nonporous-HFBMA-MAH-MIP film, which show significant morphological differences. From Fig. 1a, irregularly shaped interconnected macropores were observed. Instead, no macropore was observed for the nonporous-HFBMA-MAH-MIP film from Fig. 1b, and the surface of the film was very flat. With the porous and irregular film morphology, the surface area was enlarged and numerous imprinted sites could be generated on the inner surface. The interconnected macroporous structure is favorable of protein diffusion into the inner surface in the rebinding process, which will lead to a fast rebinding kinetics. Moreover, in comparison with other porogens, such as silica, calcium carbonate is relatively easy-to-get, low-cost and can be removed easily in moderate conditions. In addition, the thickness of the porous film fabricated here was about 10 μm as shown in Fig. S2.

The porous-HFBMA-MAH-MIP and corresponding nonporous-HFBMA-MAH-MIP films were subjected to ribonuclease A

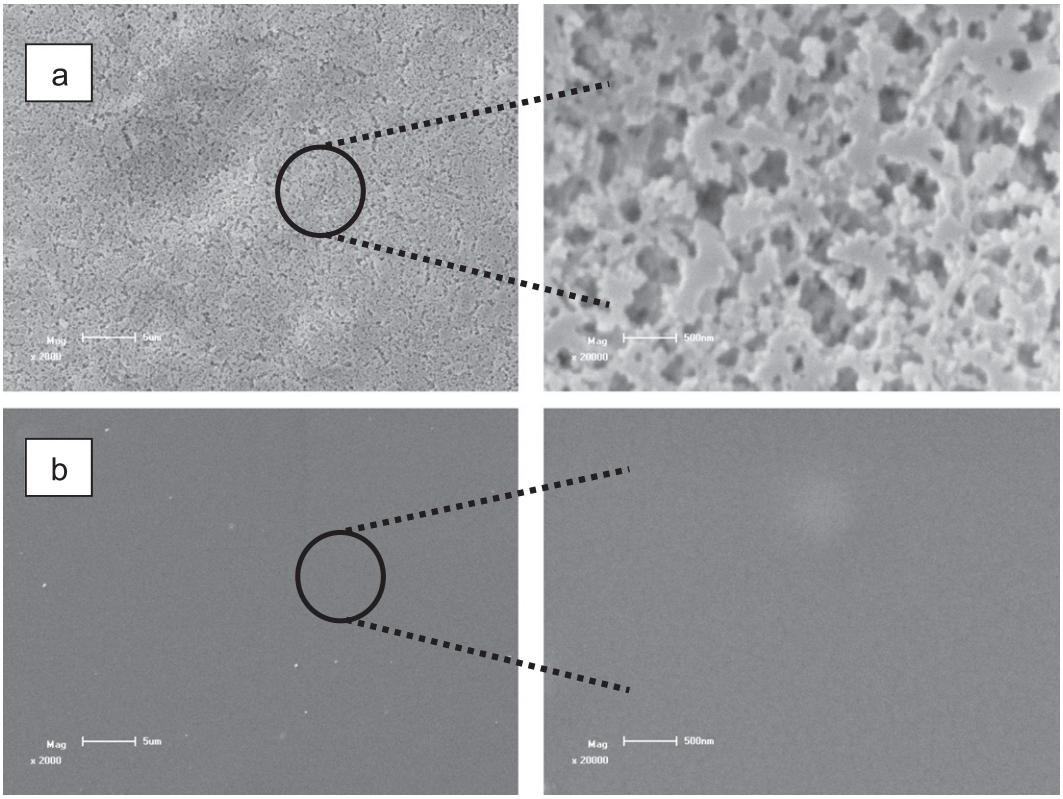

Fig. 1. The SEM images of the porous-HFBMA-MAH-MIP film (a) and nonporous-HFBMA-MAH-MIP film (b).

rebinding tests to elucidate their adsorption behaviors. For each measurement, the rebinding tests had been performed in a series of different protein solutions with concentrations from low (1×10^{-6} g/mL) to high (1×10^{-3} g/mL). As Fig. 2 showed, for both porous-HFBMA-MAH-MIP and nonporous-HFBMA-MAH-MIP films, the QCM frequency shifts increased all with the increase of the ribonuclease A concentration. For the porous-HFBMA-MAH-MIP film, 13.4 Hz frequency shift was observed under the lowest concentration of 1×10^{-6} g/mL and 60.1 Hz at maximum. For the nonporous-HFBMA-MAH-MIP film, the corresponding shifts were much smaller and just 7.5 Hz and 38.7 Hz respectively. For the nonporous-HFBMA-MAH-MIP film, the effectively imprinted area was just limited to the flat upper surface of the film. However, for the porous-HFBMA-MAH-MIP film, the frequency shifts were much larger than that of the nonporous-HFBMA-MAH-MIP film, which could attribute to the fact that the surface area of the porous film was larger, thus leading to more imprinted sites generated on the film. Moreover, the binding capacity for the porous-HFBMA-MAH-MIP film in dilute solutions was larger than that of the nonporous-HFBMA-MAH-MIP film owing to the weaker mass transport barrier. This enrichment effect would amplify the response signal intensively and enhance the detection limit of the biosensor.

3.3. Comparison of MIP and NIP films on template assay

The porous-HFBMA-MAH-MIP and porous-HFBMA-MAH-NIP films were tested to investigate the affinity of imprinted film to the template in the concentrations ranging from 1×10^{-6} g/mL to 1×10^{-3} g/mL. As shown in Fig. 3, the porous-HFBMA-MAH-MIP film exhibited a higher frequency shift for template than that of the porous-HFBMA-MAH-NIP film at the same concentration. The frequency shift due to the presence of ribonuclease A for the nonimprinted sensor turned out to be as low as 0.8 Hz under the lowest concentration of 1×10^{-6} g/mL, which could attribute to that there was no imprinted site on the polymer surface that could geometrically fit the protein and fluorinated groups could prevent protein adsorption. At this concentration, the frequency shift for the imprinted sensor was 17 times higher than that of the nonimprinted one. This result indicated that the imprinted cavities fit the size and shape of the template used for imprinting and the imprinted film had specific affinity to the template. The

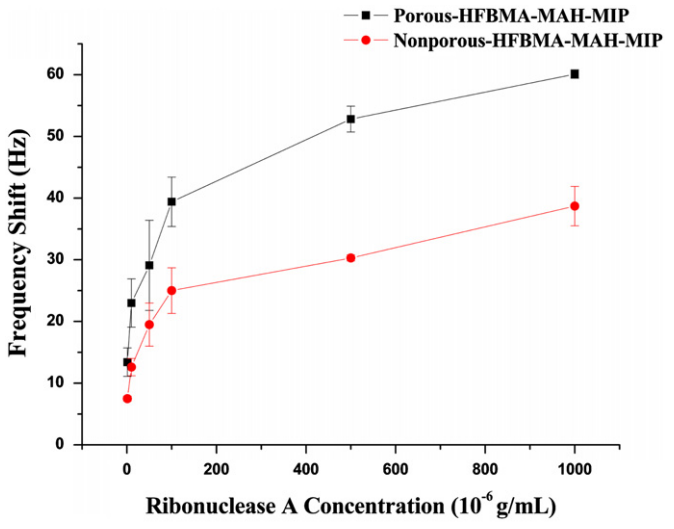

Fig. 2. The frequency shifts of the porous-HFBMA-MAH-MIP and nonporous-HFBMA-MAH-MIP films upon exposure to increasing concentrations of ribonuclease A solutions. Error bars indicate the standard deviation in triplicated experiments.

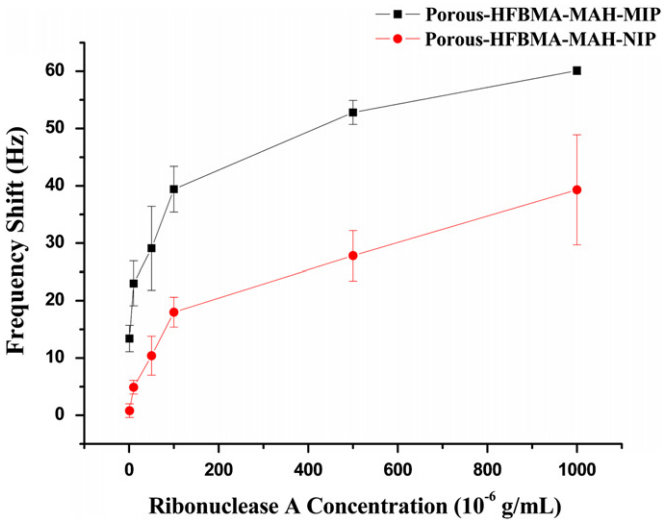

Fig. 3. The frequency shifts of the porous-HFBMA-MAH-MIP and porous-HFBMA-MAH-NIP films upon exposure to increasing concentrations of ribonuclease A solutions. Error bars indicate the standard deviation in triplicated experiments.

low adsorption of ribonuclease A for the nonimprinted film could be attributed to no specific binding site and fluorinated groups barrier.

3.4. Effect of MAH on template assay

Imprinted films with MAH as the functional monomer have stronger specific binding affinity to the target protein because of electrostatic interactions between MAH and proteins in neutral solutions. To prove this, porous-HFBMA-MAH-MIP and porous-HFBMA-MIP films were tested to investigate the affinity to the template in the concentrations ranging from 1×10^{-6} g/mL to 1×10^{-3} g/mL. As shown in Fig. 4, for the porous-HFBMA-MAH-MIP film, 13.4 Hz frequency shift was observed under the lowest concentration of 1×10^{-6} g/mL and 60.1 Hz at maximum. But for the porous-HFBMA-MIP film, the corresponding shifts were just 2.9 Hz and 42.8 Hz respectively. Obviously, the presence of MAH can enhance the adsorption capacity between matrix and proteins and the effect of MAH is outstanding especially in lower protein concentrations. The possible reason could be that because of electrostatic interactions between MAH and proteins, template could diffuse to the imprinted sites faster in dilute solutions, and thus leading to more adsorption. While in the higher template concentrations, the protein adsorption reached equilibrium slowly, which lessened the effect of MAH. In conclusion, the porous-HFBMA-MAH-MIP film exhibited a higher frequency shift for template than that of the porous-HFBMA-MIP film at the same concentration, indicating the enhanced specific adsorption from the introduction of MAH.

3.5. Effect of HFBMA to the selectivity

Selectivity is a key parameter in preparing molecularly imprinted polymers. In order to probe the selectivity and specificity of the biosensor to the target protein, lysozyme was employed as the control protein for the selectivity tests because of its similar molecular size and weight with ribonuclease A. As Table 1 showed, for the porous-HFBMA-MAH-MIP film, under the same series of concentrations determined, frequency shifts for ribonuclease A increase from 13.4 Hz to 60.1 Hz, while for the control lysozyme, the frequency shifts were 4.1 Hz and 49.7 Hz respectively. The imprinting selectivity factors were 3.3 under the concentrations of 1×10^{-6} g/mL, and above 2.0 for the other three

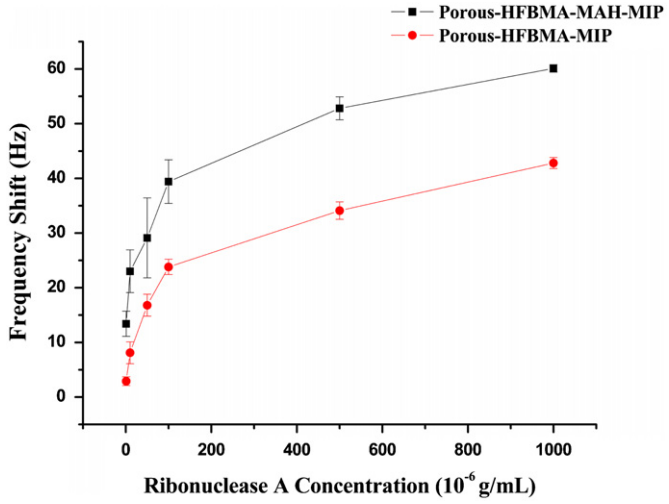

Fig. 4. The frequency shifts of the porous-HFBMA-MAH-MIP and porous-HFBMA-MIP films upon exposure to increasing concentrations of ribonuclease A solutions. Error bars indicate the standard deviation in triplicated experiments.

low concentrations (1×10^{-5}, 5×10^{-5}, 1×10^{-4} g/mL). This was mainly because that lysozyme was not shape complementary to the ribonuclease A imprinted cavities, and the frequency shifts for lysozyme arose from the nonspecific adsorption. But for the template protein, numerous ribonuclease A imprinted cavities were generated on the surface of the macropores in the film fabrication process, thus specific adsorption to template in dilute solutions was mainly through the synergistic effect of shape complementary and electrostatic interactions during the recognition process. But in higher concentrations, more and more imprinted cavities were occupied, thus leading to more nonspecific adsorption. So the imprinting selectivity factors became much smaller as the concentration increased.

To prove whether the fluoromonomer introduced into the imprinted film could lessen the nonspecific adsorption, the porous-BMA-MAH-MIP film was tested upon exposure to increasing concentrations of template and control protein. As shown in Table 1, the frequency shifts for porous-HFBMA-MAH-MIP film were much smaller than the porous-BMA-MAH-MIP film in a series of concentrations of lysozyme. The frequency shifts for lysozyme arose mainly due to the nonspecific adsorption, so fluorinated groups could lessen the nonspecific binding as we expected. The frequency shifts for the two films were nearly the same in the three low concentrations (1×10^{-6}, 1×10^{-5}, 5×10^{-5} g/mL) for ribonuclease A assays. While in dilute solutions, the frequency response to the template was mainly due to specific adsorption, thus illuminating that fluorinated groups had a less influence to specific binding than acrylate based matrix. In all, the introduction of fluorinated monomer had the effect of reducing nonspecific adsorption of proteins. Consequently, the imprinting selectivity factors of the porous-HFBMA-MAH-MIP film were much larger than that of porous-BMA-MAH-MIP film (Table 1).

3.6. *Response feature*

The rapid response to external stimuli which endows the biosensors with real-time detection functionality is very significant. In general, the response time is only several seconds for small molecules, whereas for biomacromolecules such as proteins, the response time is usually several or tens of minutes because of the slow diffusion from bulk solution to recognition sites. In our previous work (Zhou et al., 2011), films based on QCM were designed with only acrylate based polymer, and the response time was about 10 min. The response of the biosensor based on this work and exposed to a series of concentrations of ribonuclease A was shown in Fig. S3, indicating a rapid response time for about 1 min. This result can be explained that on one hand the interconnected macroporous structure is favorable of the diffusion of protein macromolecules to the imprinted cavities, and on the other hand electrostatic interactions between MAH and proteins make it fast to reach the adsorption equilibrium. The rapid response and short equilibrium-attainment time features endow the biosensor with real-time functionality.

Table 1
The oscillation frequency shifts of the porous-HFBMA-MAH-MIP and porous-BMA-MAH-MIP porous films upon exposure to increasing concentrations of ribonuclease A and lysozyme solutions ($\pm$SD, $n=3$).

C(g/mL)	Porous-HFBMA-MAH-MIP			Porous-BMA-MAH-MIP		
	Δf (Hz)			Δf (Hz)		
	ribonuclease A	lysozyme	SF	ribonuclease A	lysozyme	SF
1×10^{-6}	13.4 ± 2.3	4.1 ± 1.6	3.3	12.2 ± 3.1	7.8 ± 1.7	1.6
1×10^{-5}	23.0 ± 3.9	9.2 ± 1.1	2.5	21.8 ± 2.8	15.0 ± 1.8	1.4
5×10^{-5}	29.1 ± 7.3	14.1 ± 3.2	2.1	32.0 ± 0.6	22.2 ± 2.1	1.4
1×10^{-4}	39.4 ± 4.0	17.3 ± 3.5	2.3	45.3 ± 2.1	27.6 ± 2.0	1.6
5×10^{-4}	52.8 ± 2.1	33.1 ± 3.5	1.6	63.2 ± 2.6	48.6 ± 1.7	1.3
1×10^{-3}	60.1 ± 0.7	49.7 ± 5.6	1.2	79.3 ± 4.8	64.4 ± 2.8	1.2

In addition, for different films, each of ribonuclease A and lysozyme was tested 3 times, and the deviations were small as Table 1 showed, indicating that the QCM sensor still worked efficiently after 6 times of recycled measurements, and the films were durable in the tested aqueous condition. The frequency shift for ribonuclease A was 59.5 Hz after continuous injection of the template in different concentrations, which was 60.0 Hz after 2 months for the porous-HFBMA-MAH-MIP film, so the QCM sensor fabricated in our lab could be stored for 2 months or more.

4. Conclusion

In this work, we have fabricated a novel macroporous protein imprinted film based on QCM using MAH as the functional monomer and HFBMA as the matrix monomer. The surface area of the biosensor was effectively enlarged by employing calcium carbonate nanoparticles as the porogen. The specific binding affinity to the target protein ribonuclease A was enhanced because of electrostatic interactions between MAH and proteins in neutral solutions. Simultaneously, fluoromonomer HFBMA can reduce the nonspecific protein adsorption, which leads to a larger selectivity factor. The biosensor is specific, selective and fast response to dilute ribonuclease A solutions. The strategy proposed here has great promise to create devices for high performance protein detection in aqueous environment.

Acknowledgments

We gratefully acknowledge the support of the National Natural Science Foundation of China (Proj. nos. 20874052 and 50978138).

Appendix A. Supporting information

Supplementary data associated with this article can be found in the online version at http://dx.doi.org/10.1016/j.bios.2012.11.002.

References

Aizawa, H., Kurosawa, S., Tozuka, M., Prak, J.W., Kobayashi, K., 2004. Sensors and Actuators B 101, 150–154.

Bossi, A., Bonini, F., Turner, A.P.F., Piletsky, S.A., 2007. Biosensors and Bioelectronics 22, 1131–1137.

Bures, P., Huang, Y., Oral, E., Peppas, N.A., 2011. Journal of Controlled Release 72, 25–33.

Byren, R., Dianmond, D., 2006. Nature Materials 5, 421–424.

Cui, L., Swann, M., Glidle, A., Barker, J., Cooper, J.M., 2000. Sensors and Actuators B 66, 94–97.

Cutivet, A., Schembri, C., Kovensky, J., Haupt, K., 2009. Journal of the American Chemical Society 131, 14699–14702.

Ding, B., Wang, X.F., Yu, J.Y., Wang, M., 2011. Journal of Materials Chemistry 21, 12784–12792.

Ernsting, M.J., Labow, R.S., Santerre, J.P., 2007. Journal of Biomedical Materials Research 3, 759–769.

Guo, T.Y., Xia, Y.Q., Hao, G.J., Song, M.D., Zhang, B.H., 2004. Biomaterials 25, 5905–5912.

Hua, K.C., Zhang, L., Zhang, Z.H., Guo, Y., Guo, T.Y., 2011. Acta Biomaterialia 7, 3086–3093.

Jonsson, M.P., Jonsson, P., Hook, F., 2008. Analytical Chemistry 80, 7988–7995.

Kwon, S., Kim, H., Ha., J.W., Lee, S.Y., 2011. Journal of Industrial and Engineering Chemistry 17, 259–263.

Lee, M.H., James, L., 2011. ACS Applied Materials & Interfaces 3, 3064–3071.

Li, J., Jiang, F., Li, Y., Chen, Z., 2011. Biosensors and Bioelectronics 26, 2097–2101.

Liu, G.Q., Li, X.L., Xiong, S.D., 2012. Journal of Fluorine Chemistry 135, 75–82.

Lu, C.H., Zhang, Y., Tang, S.F., et al., 2012. Biosensors and Bioelectronics 31, 439–444.

Pernites, R., Ponnapati, R., Felipe, M.J., Advincula, R., 2011. Biosensors and Bioelectronics 26, 2766–2771.

Potyrailo, R.A., 2006. Angewandte Chemie—International Edition 45, 702.

Say, R., Garipcan, B., Emir, S., Patlr, S., Denizli, A., 2002. Colloids and Surfaces A: Physicochemical and Engineering Aspects 196, 199.

Sellergren, B., Allender, C.J., 2005. Advanced Drug Delivery Reviews 57, 1733.

Tan, C.J., Tong, Y.W., 2007. Langmuir 23, 2722–2730.

Tan, C.J., Wangrangsimakul, S., Bai, R., Tong, Y.W., 2008. Chemistry of Materials 20, 118–127.

Tatemichi, M., Sakamoto, M., Mizuhata, M., Deki, S., Takeuchi, T., 2007. Journal of the American Chemical Society 129, 10906–10910.

Wang, H.J., Zhou, W.H., Yin, X.F., Zhuang, Z.X., Yang, H.H., Wang, X.R., 2006. Journal of the American Chemical Society 128, 15954–15955.

Xia, Y.Q., Guo, T.Y., Song, M.D., Zhang, B.H., Zhang, B.L., 2005. Biomacromolecules 6, 2601–2606.

Yang, H., Guo, T.Y., Zhou, D.Z., 2011. International Journal of Biological Macromolecules 48, 432–438.

Yano, K., Karube, I., 1999. Trends in Analytical Chemistry 8, 199–204.

Zhang, W., He, X.W., Chen, Y., Li, W.Y., Zhang, Y.K., 2011. Biosensors and Bioelectronics 26, 2553–2558.

Zhang, Z.H., Hu, Y.L., Liu, Z.S., Guo, T.Y., 2012. Polymer 53, 2979–2990.

Zheng, J.B., Li, G., Ma, X.F., Wang, Y.M., Wu, G., Cheng, Y.N., 2008. Sensors and Actuators B 133, 374–380.

Zhou, D.Z., Guo, T.Y., Yang, Y., Zhang, Z.P., 2011. Sensors and Actuators B 153, 96–102.